

Upconversion luminescence of CdTe nanoparticlesAlan G. Joly,¹ Wei Chen,^{2,*} David E. McCready,¹ Jan-Olle Malm,³ and Jan-Olov Bovin³¹*Pacific Northwest National Laboratory, P.O. Box 999, Richland, Washington 99352, USA*²*Nomadics, Inc., 1024 South Innovation Way, Stillwater, Oklahoma 74074, USA*³*Materials Chemistry, Center for Chemistry and Chemical Engineering, Lund University, P.O. Box 124, SE-22100, Lund, Sweden*

(Received 5 July 2004; revised manuscript received 1 November 2004; published 6 April 2005)

Efficient upconversion luminescence is observed from CdTe nanoparticles in solution and precipitated as solids. In the solids, the upconversion luminescence spectrum is significantly red shifted relative to the photoluminescence spectrum, whereas in solution, there is very little spectral shift. The upconversion luminescence exhibits a near-quadratic laser power dependence, both at room temperature and at 10 K. Both the upconversion and photoluminescence show similar decay dynamics with the solid samples showing shorter lifetimes compared to the solutions. This lifetime shortening is attributed to surface-state quenching. These results indicate that two-photon excitation is the likely upconversion excitation mechanism in these particles and that phonon-populated trap states do not contribute to the upconversion.

DOI: 10.1103/PhysRevB.71.165304

PACS number(s): 78.55.Et

I. INTRODUCTION

Recent interest in a number of applications including laser technology,¹ three-dimensional microfabrication and optical storage,^{2,3} displays and optical limiting,⁴ imaging techniques,⁵ and biological caging⁶ has renewed interest in upconversion luminescence.⁷ Upconversion luminescence (UCL) is luminescence in which the emitted wavelength is shorter (higher in energy) than the excitation wavelength in contrast to photoluminescence (PL), where the emitted wavelength is lower in energy than the excitation photons. Upconversion luminescence has been readily observed in bulk semiconductors such as ZnS:Mn²⁺ (Ref. 8) as well as in porous silicon,^{9–11} CdS nanoparticles,^{12,13} CdTe,^{14–16} CdSe and InP colloidal nanoparticles,¹⁷ CdSe/ZnS quantum dots,^{18,19} and III-V quantum dots.^{20–23}

Auger recombination,^{10,22} two-photon absorption,^{12,13,21,23} and thermally assisted surface-state processes^{14–19} have been proposed to explain these observations. The Auger process involves transfer of energy from an excited electron-hole pair upon recombination to another electron or hole, creating a highly excited carrier. This carrier is then available for recombination at a higher energy than the original excitation wavelength. Two-photon absorption may occur in one of two ways: The process may proceed through an intermediate state within the band gap and is then termed two-step two-photon absorption (TSTPA) or else the process may proceed through a virtual intermediate state (TPA). The process occurring with a virtual intermediate state is significantly weaker and often requires higher excitation powers. Both the Auger and TPA processes are inherently nonlinear in nature, requiring the initial photon to populate an intermediate state and then excitation of this intermediate state to a higher excited state via either Auger or a second photon excitation. Upconversion via surface-state processes involves thermally populated defect states which absorb a single photon, leading to higher-energy luminescence. These processes show single-photon power dependences and a temperature dependence characterized by increasing UCL intensity at increasing temperatures. These processes are also extremely efficient, often

only requiring a continuous-wave (cw) source such as a He-Ne laser or a Xe lamp.

Nanoparticles or quantum dots have the potential to become a new class of fluorescent probes for many biological and biomedical applications, especially cellular imaging.^{24–29} Many recent publications have been dedicated to the applications of luminescent nanoparticles for biological or biomedical imaging or probing.^{24–29} In these reports, the luminescence images are recorded with an optical microscope or a confocal microscope based on nanoparticle fluorescence.^{26–29} For biological applications, upconversion luminescence techniques have several advantages over fluorescence because autofluorescence (background luminescence from cell proteins) can be avoided using upconversion measurements.⁵ Consequently, more sensitive and higher-resolution imaging or detection may be obtained. Upconversion luminescence of nanoparticles also has the potential to be useful in display technology, as well as memory and lighting applications. Thus, new materials and techniques for understanding the underlying physics of these processes is extremely valuable.

In this paper, we report our new observations on the upconversion luminescence of CdTe nanoparticle solid and solution samples based on the measurements of the power dependence and decay dynamics. Our observations reveal that the upconversion luminescence in the solution and solid samples occurs by two-photon excitation. In the solid samples, the upconversion luminescence contains a greater contribution from either larger particles or surface states relative to the photoluminescence.

II. EXPERIMENT

Cadmium perchlorate hydrate (Aldrich), aluminum telluride (99.5% pure, Gerac), thioglycolic (mercaptoacetic) acid (Aldrich), L-cysteine (99% pure, Alfa), and sulfuric acid (95% pure, Aldrich) were used as received. CdTe nanoparticles were prepared by the reaction of precursors containing cadmium perchlorate hydrate and hydrogen telluride (H₂Te)

under vigorous stirring. The Cd^{2+} -containing solution was prepared as follows: 0.7311 g of $\text{Cd}(\text{ClO}_4)_2 \cdot \text{H}_2\text{O}$ was dissolved in 125 ml of water. Then 0.25 ml of thioglycolic acid (TGA) or 0.4 g of L-cysteine was added to the solution and the pH adjusted to ~ 11 by the addition of 0.1 Mol NaOH. The solution was then purged with nitrogen for at least 30 min. H_2Te gas was generated by the chemical reaction of excess aluminum telluride with 0.5 Mol sulfuric acid in an inert atmosphere (nitrogen) and was combined with the above solution containing Cd^{2+} ions using the setup as described in Ref. 30. After the completion of the reaction a yellow (TGA) or green (L-cysteine) solution of CdTe nanocrystal nuclei was obtained. This solution was then refluxed at 100 °C to promote crystal growth. During the growth process, fractions with nanoparticles of different sizes were extracted and stored at 4 °C in the dark. The solid samples were made from the solution by adding acetone and the precipitation was carried out at 4 °C in order to avoid oxidation of the nanoparticles. The experiments in this paper were carried out on two solution samples (orange and green) and three solid samples (yellow, orange, and red).

The phase identity and average crystallite size of the nanoparticles were determined by x-ray powder diffraction (XRPD) and high-resolution transmission electron microscopy (HRTEM). The diffraction apparatus was a Philips X'Pert MRD system (PW3040/00 type) equipped with variable slits and a Cu x-ray source ($\lambda = 0.15406$ nm) operated at 1.8 kV. The study specimens were ground in an agate mortar and pestle, then mounted in an off-axis quartz (001), front-loading, cavity-type holder which produced minimal background signal. The XRPD scan range was 10.00° – 80.00° 2θ and the scan rate varied from 0.6 to $1.5^\circ/\text{min}$. Analysis of the experimental XRPD patterns was accomplished using the program JADE (Materials Data, Inc., Livermore, CA) and the Powder Diffraction File database (International Centre for Diffraction Data, Newtown Square, PA). The nanoparticles in solution were brought onto holey carbon-covered copper grids for HRTEM observations. The HRTEM images of the particles were obtained with an electron microscope (400 kV) with a structural resolution of 0.16 nm.

Room-temperature optical absorption spectra were taken with a Hewlett-Packard HP8453 spectrophotometer. The photoluminescence excitation and emission were recorded on a SPEX FLUOROLOG fluorescence spectrophotometer. The upconversion emission spectra and power dependences were collected using a nanosecond optical parametric oscillator and amplifier (Spectra-Physics MOPO-730) operating at a 10-Hz repetition rate and tunable between 440 nm and 1800 nm. The laser output was directed onto the particles and emission was collected at right angles to the excitation and focused into a 1/8-m monochromator equipped with a gated-intensified charge-coupled-device (CCD) detector. The power dependences were measured by integrating the area under the luminescence as a function of input power. The lifetimes were collected using the output of a femtosecond regeneratively amplified titanium:sapphire laser system operating at 1 kHz. The 150-fs pulses of this laser at either 830 nm (for upconversion luminescence) or else the second harmonic at 415 nm

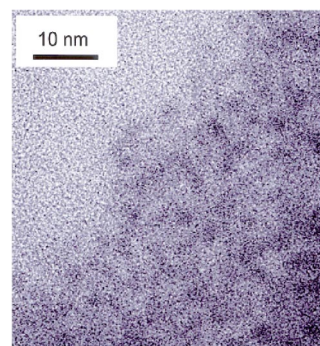


FIG. 1. HRTEM image of CdTe nanoparticles orange particles showing an average size between 3 and 4 nm.

(for photoluminescence) was directed onto the particles and the emission was collected at right angles and focused into a streak camera (Hamamatsu C5680). Suitable bandpass and cutoff filters were used to collect the luminescence at different wavelengths. The time resolution was determined to be about 200 ps full width at half maximum (FWHM) using a standard scattering material.

III. RESULTS AND DISCUSSION

A. Solution samples

The methods for making CdTe nanoparticles are well developed. The sizes of the particles in this paper were controlled by the reaction time as described in Refs. 30–32. To confirm the formation of CdTe nanoparticles, HRTEM images were used to observe the structure, size, and shape of the particles. The particle size of the orange nanoparticle solution sample is around 3–4 nm, as estimated from HRTEM images (Fig. 1). As observed in Fig. 1, most nanoparticles are spherical in shape. The [111] lattice spacing of the particles is estimated to be about 0.36 nm from the HRTEM images. This is in good agreement with the [111] spacing of cubic CdTe [0.374 nm (Ref. 33)].

Figure 2 displays the absorption, photoluminescence, and upconversion emission spectra of the green and orange solution samples. Both the green and the orange solutions have

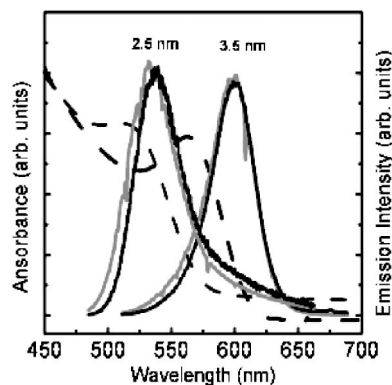


FIG. 2. Optical absorption (dashed line), photoluminescence emission (gray line), and upconversion emission (black line) of green (2.5 nm) and orange (3.5 nm) CdTe particle solutions.

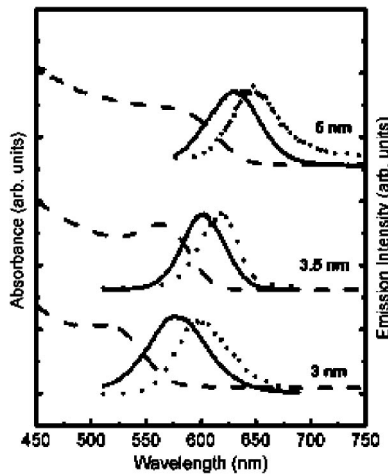


FIG. 3. Optical absorption (dashed line), photoluminescence emission (solid line), and upconversion emission (dotted line) of the yellow (3 nm), orange (3.5 nm), and red (5 nm) CdTe particle solid samples.

pronounced absorption peaking at 515 nm and 563 nm, respectively, which are blueshifted from the energy gap of bulk CdTe [860 nm (Ref. 34)]. The absorption maximum and edges shift to shorter wavelengths with decreasing size as a consequence of quantum size confinement. The sizes of the nanoparticles may be estimated using the effective mass approximation³⁵ and the shift of the absorption edge. The particle sizes are estimated to be around 2.5 nm for the green and 3.5 nm for the orange solutions, respectively, which are in good agreement with the results from HRTEM measurements.

The photoluminescence and upconversion luminescence spectra are also displayed in Fig. 2. The PL of the green solution peaks at 532 nm and the UCL peaks at 537 nm, 5 nm redshifted from the PL emission maximum. For the orange solution, both the PL and UCL have emission maxima at the same wavelength, 600 nm.

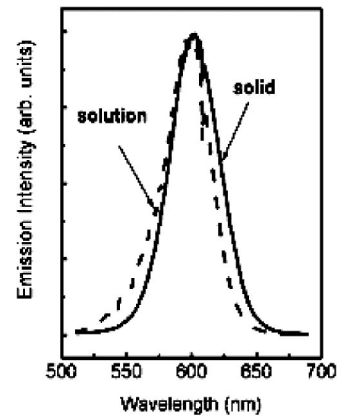
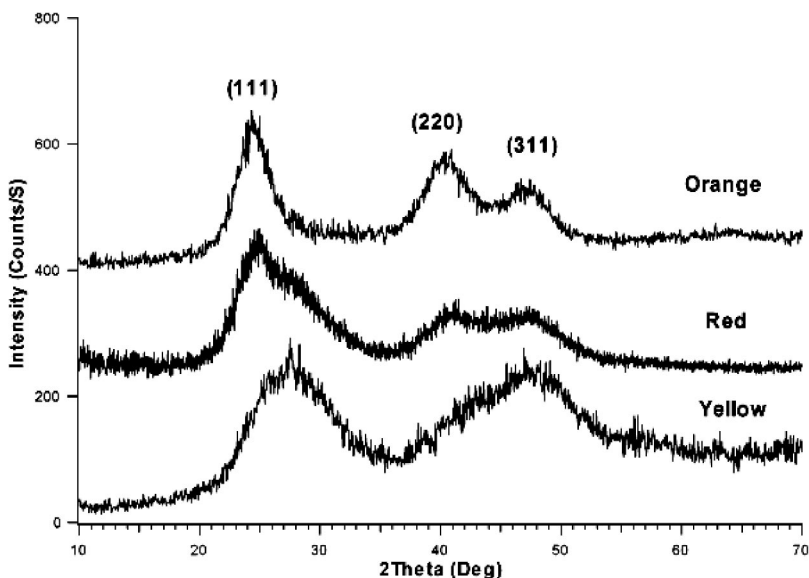


FIG. 4. Photoluminescence emission spectra of the orange CdTe particle solution (dash) and solid (solid) samples.

B. Solid samples

Figure 3 displays the photoluminescence and upconversion luminescence spectra of the three solid samples (yellow, orange, and red) along with the absorption spectra of the solution samples from which the solid samples were precipitated. All three solutions have pronounced absorptions peaking at 522 nm, 563 nm, and 585 nm, which are blueshifted from the energy gap of bulk CdTe at 860 nm (Ref. 34) as a result of quantum size confinement. Accordingly, the particle sizes are estimated to be around 3, 3.5, and 5 nm for the three samples.

The orange solid sample precipitated from solution displays a PL spectrum almost identical to the orange solution (Fig. 4). However, in the solid sample the upconversion luminescence maximum is about 16 nm redshifted from that of the photoluminescence emission maximum, unlike the solution sample which shows a negligible difference between the PL and UCL emission spectra. Similar results are observed for the yellow and red solid samples. For the yellow sample, the upconversion luminescence is about 21.5 nm and for the red solid sample the upconversion emission is about 17 nm

FIG. 5. X-ray powder diffraction patterns of the orange, red, and yellow CdTe particle solid samples.

TABLE I. Absorption (ABS), photoluminescence (PL), and upconversion luminescence (UCL) peaks of CdTe nanoparticles.

Samples	Size (nm)	ABS (nm)	PL (nm)	UCL(nm)	Stokes (nm)	PL-UCL(nm)
Green solution	2.5	515	532	537	17	5
Orange solution	3.5	563	600	600	37	0
Yellow solid	3	522	577	598.5	55	21.5
Orange solid	3.5	563	602	618	39	17
Red solid	5	585	630	647	45	17

redshifted from that of the photoluminescence emission maximum.

The emission spectrum of the solid orange sample is almost identical to that of the solution sample. This indicates that the particle size in the solid sample is similar to the particle size in the solution from which the solid sample is precipitated. For the solid samples the upconversion emission peak is significantly more redshifted from the photoluminescence emission peak than for the solution samples. In order to better understand the nature of the solid samples, x-ray powder diffraction measurements were performed on the three samples. Figure 5 shows the XRPD patterns of the orange, red, and yellow solid samples. Three reflection peaks corresponding to the (111), (220), and (311) planes of cubic zinc-blende CdTe (PDF No. 15-770) are observed. While the XRPD results give information about the average crystallite size, this is not necessarily the same as the particle size. It is

commonly accepted that in CdTe nanoparticles, larger particles show emission at longer (redder) wavelengths and smaller particles emit at shorter wavelengths.^{30-32,35,36} In addition, the HRTEM measurement provides information about the particle size that corresponds well with the optical measurements. From the XRPD results, the samples are observed to have varying degrees of crystallinity. The orange particles show the highest degree of crystallinity with an average crystallite size of about 2.3 nm. This is similar to the particle size as determined by HRTEM and optical measurements and implies that the particles are mostly single phase. The red particles display both a weakly crystalline component and a broader background. The broad background arises from particles with crystallite sizes smaller than the particle size; therefore, the particles cannot be considered single phase although they still retain a degree of crystallinity. The yellow particles show only broad diffraction peaks; therefore, the average crystal domain size is significantly less than the particle diameter. From these measurements, we can conclude that the orange particles are mostly monocrystalline, the red particles are less crystalline, and the yellow particles are the least crystalline. Thus, although Scherrer's equation predicts

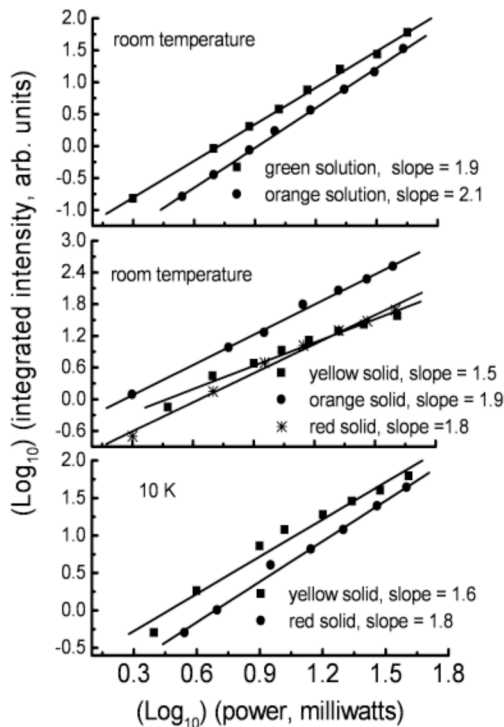


FIG. 6. A semilogarithmic base of 10 (\log_{10}) plot of the power dependences of the upconversion emission intensity on laser power at both room temperature and 10 K for CdTe solution and solid samples.

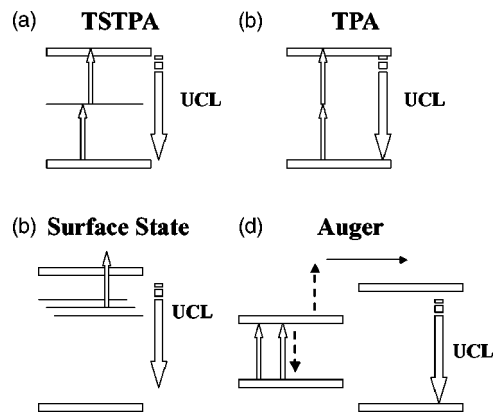


FIG. 7. A schematic illustration of various processes that result in upconversion of the incident photons. (a) represents two-step two-photon absorption through a real intermediate state while (b) represents two-photon absorption through a virtual intermediate. (c) displays upconversion from thermally populated intragap states. (d) Auger-type upconversion requires two excited carriers which may interact such that the energy of recombination of the first excited carrier is transferred to the other excited carrier. This carrier may then diffuse to a different region (material) in a heterostructure and result in luminescence with an energy characteristic of the larger band-gap material.

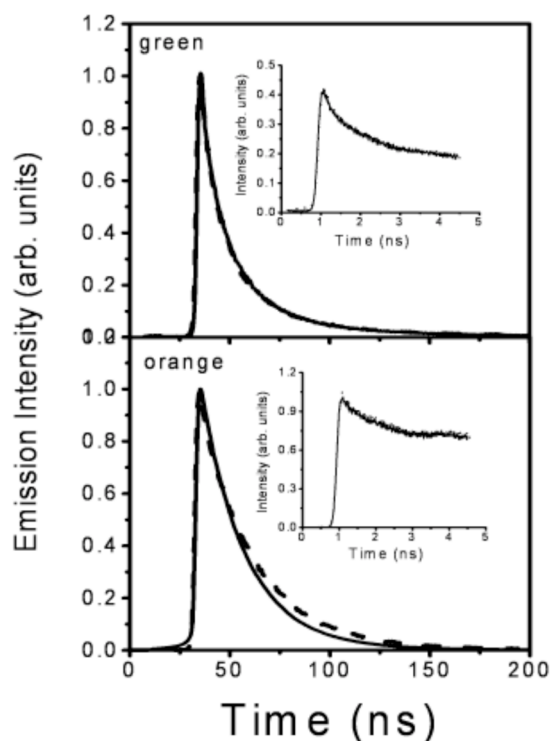


FIG. 8. Photoluminescence (solid line, excited at 403 nm) and upconversion (dashed line, excited at 805 nm) decay curves of green and orange CdTe nanoparticle solutions.

that the smallest crystallites should have the broadest diffraction peaks,³⁷ it cannot be used to give reliable values for particle size because of the varying degrees of crystallinity of the different samples.

Interestingly, the conclusion from the XRPD measurements is in agreement with the optical observations. The Stokes shift of the emission maximum from the absorption peak is a parameter that can reflect the particle quality. Generally, the Stokes shift is greater if the nanoparticles contain a higher concentration of surface states or defects because these surface states or defects are often the origin of the luminescence and shift the emission to longer wavelength.³⁶ As shown in Table I, the yellow sample has a larger Stokes shift (55 nm) than the red sample (45 nm) and the red sample has a larger Stokes shift than the orange sample (39 nm). This is consistent with the conclusion from the XRPD observations.

C. Upconversion mechanism

Several publications have been dedicated to the upconversion from semiconductor nanoparticles; however, the mechanisms for upconversion luminescence in semiconductor nanoparticles are still under debate. Often the dependence of the UCL on the input photon power dependence can yield some insight into the mechanism. A semilogarithmic plot displaying the excitation laser power dependences of the upconversion luminescence intensity are displayed in Fig. 6 for the green solution, orange solution, yellow solid, orange solid, and red solid samples, respectively. The excitation laser

power dependences were performed over one order of magnitude, beginning at the detection limit on the low-power end. Using the relation of $I \sim \text{power}^K$, where I is the intensity of the luminescence and “power” represents the input laser excitation power, the values of K are about 1.9–2.1 for the solution samples and are 1.5–1.9 for the solid samples. Therefore the UCL mechanism is largely two-photon in nature, although the yellow solid particles show some variation. Figure 7 displays mechanisms commonly employed to explain upconversion luminescence in nanostructured systems. Both TSTPA and TSA [Figs. 7(a) and 7(b)] are expected to show a quadratic power dependence as observed here. In recent investigations of UCL in CdTe nanoparticles, a linear excitation laser power dependence of the UCL intensity was observed.^{14–16} In addition, extremely low excitation powers were used to excite the UCL and the UCL in these particles increased with increasing temperature. From these observations, the authors concluded that the UCL originates in thermally populated surface states^{14–16} schematically depicted in Fig. 7(c). Auger-type excitation processes as depicted in Fig. 7(d) may also lead to a quadratic power dependence on the incident photon power. The Auger-type process is essentially an energy transfer process between an excited electron-hole pair and a second excited carrier. The energy from recombination of the excited electron-hole pair may be transferred to the second excited carrier, resulting in an increase of this carrier’s energy. This carrier is then available for recombination resulting in luminescence at a higher energy than the input photon.

Auger-type upconversion occurs most frequently in heterostructures or quantum well systems. This process requires that the incident photon energy span the band gap of at least one of the materials to form excitons in the smaller-band-gap material [Fig. 7(d)]. The Auger process results in a high-energy carrier that can diffuse to the larger-band-gap material where it can result in frequency upconverted luminescence from the larger-band-gap material [Fig. 7(d)]. Such a mechanism has been used to explain UCL in GaAs-GaInP₂ interfaces.²² Quadratic Auger-type processes require that electron-hole pairs be formed with the initial photon. In the CdTe nanoparticles reported here, the incident photons are not energetic enough to produce electron-hole pairs or excitons. Therefore, Auger-type processes may be ruled out as a possible mechanism to explain the observed upconversion.

Although the solution power dependences are quadratic, the solids show a slightly smaller value. The nonquadratic power dependences may result from either competition between linear and quadratic processes or else saturation of the nonlinear process. Linear processes as depicted in Fig. 7(c) require the participation of phonons to result in upconverted photons. In order to check whether the UCL arises from phonon populated states, the power dependences of the yellow and red samples were measured at 10 K and are displayed in Fig. 6. No variation in the power law is observed at this temperature and the UCL intensity is observed to increase at lower temperatures, leading to the conclusion that phonon-populated states do not contribute to the UCL as has been reported in other CdTe nanoparticles.^{14–16} Therefore, it is likely that the slightly lower-than-quadratic power depen-

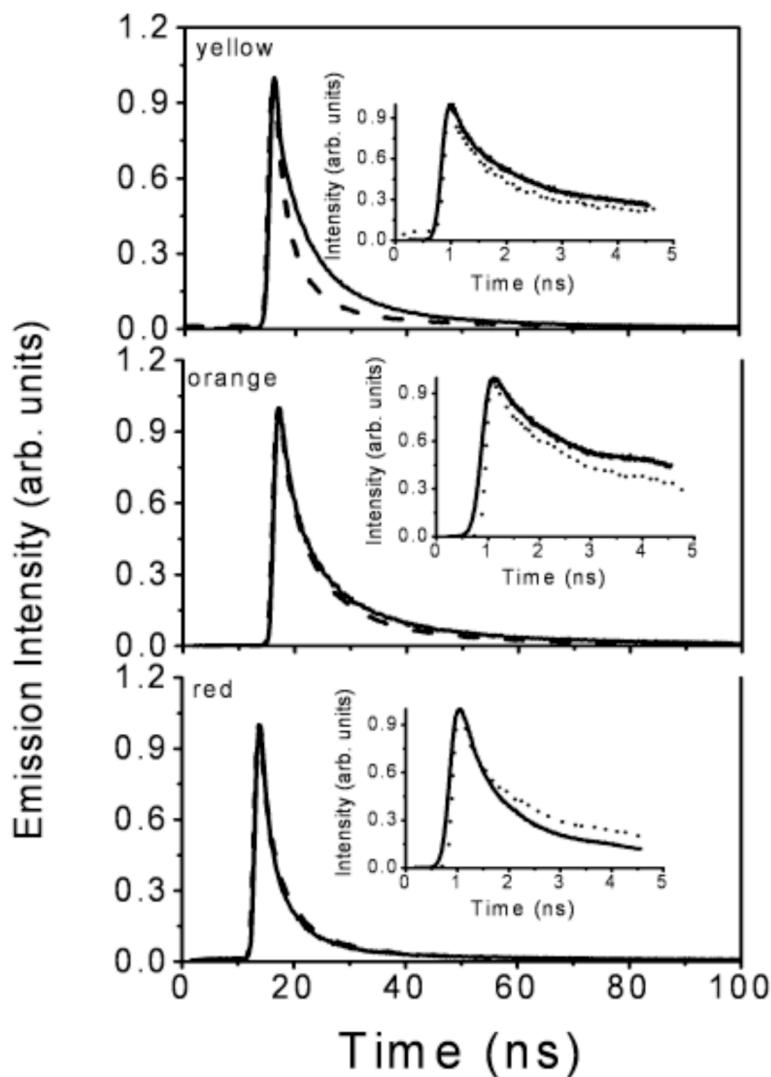


FIG. 9. Photoluminescence (solid line, excited at 403 nm) and upconversion (dashed line, excited at 805 nm) decay curves of yellow, orange, and red CdTe particle solid samples.

dences in some of the solid samples originates from saturation of the nonlinear excitation. Semiconductor nanoparticles such as CdSe-ZnS are known to have extremely large two-photon cross sections and therefore saturate extremely easily.³⁸ Attempts to reduce the input laser power in order to avoid saturation resulted in undetectable signal levels. Therefore it is reasonable to conclude that the slightly smaller-than-quadratic power dependences are due to saturation of a two-photon excitation.

Two-photon excitation may be accomplished through a real midgap state or else through a virtual intermediate state. Both processes would show similar quadratic laser power dependences. In TSTPA, the excitation process is determined by the combined excitation cross sections of the excitation from the ground state to the intermediate state and the excitation from the intermediate state to the final state. The overall excitation efficiency is governed by these cross sections and the lifetime of the intermediate state. Because the intermediate state lifetime can be fairly long (nsec, μ sec, or even msec), TSTPA can usually be accomplished with low-average-power continuous-wave laser systems. In contrast, TPA requires high peak power

because the virtual intermediate state has an extremely short lifetime (fsec) and a large number of photons/sec is required to achieve excitation. Therefore, short pulses (nsec, psec, or fsec) are usually needed to accomplish efficient excitation.

In order to ascertain whether the excitation is through a real or virtual state, the UCL from the CdTe solutions was measured under both cw and fsec-pulsed conditions using the same excitation wavelength in both cases. Following fsec-pulsed excitation, the UCL is easily observable; however, following cw excitation, no detectable UCL was observed from any of the CdTe samples investigated. Therefore, it is reasonable to conclude that the excitation mechanism is through two-photon excitation via a virtual intermediate state.

Luminescence lifetimes of both the PL and UCL measured at or near the peak emission are displayed in Figs. 8 and 9, with the results tabulated in Table II. The lifetimes reported in Table II for the solid samples are the longest-decay-component result of multiexponential fitting to the decay curves. In addition to this component, decay lifetimes on the picosecond (\sim 200 psec) time scale as well as intermedi-

TABLE II. Luminescence and upconversion lifetimes of CdTe nanoparticles.

Samples	Size (nm)	PL Lifetime ^a (nsec)	UCL Lifetime ^a (nsec)
Green solution	2.5	32	31
Orange solution	3.5	23	27
Yellow solid	3	16	16
Orange solid	3.5	3.5	2
Red solid	5	14	14

^aLifetime reported is the result of fitting the longest exponential decay of the data.

ate nsec components are present in some of the samples. In general, the luminescence from the solution samples is nearly single exponential, whereas the luminescence from the solid samples is biexponential or multiexponential. This is likely because the solid particles have less passivated surfaces due to the removal of some of the stabilizers as a result of adding acetone during the precipitation. Multiexponential behavior is often interpreted as arising from either a distribution of decay times or else to a combination of recombination from band-edge states, trap states, and surface states. In any case, the influence of surface and defect states likely results in the highly nonexponential nature of the solid-sample decay curves.

Perhaps the most significant lifetime results are the differences between the solution and solid samples and the significant shortening in the orange solid-sample lifetime relative to the other particles. Recent results also confirm lifetimes between 1 and 30 nsec for CdTe nanoparticles in solution.^{39,40} The shortening of the solid lifetimes relative to solution may be due to a higher density of surface states present in the solid samples. The additional shortening of the orange solid lifetime is not clear. Bulk indium-doped single crystal CdTe has a very short lifetime, on the order of 200 psec (Ref. 41). The orange sample is the most crystalline of the samples as demonstrated by the XRPD measurements. This may be the reason that the lifetime is significantly shorter in this sample.

For the CdTe nanoparticle solid samples, the emission lifetimes excited at 403 nm are almost identical as those obtained at one-half the excitation energy (805 nm excitation). (Fig. 9 and Table II). These results along with the power dependence favor the mechanism of two-photon absorption for the quadratic energy contribution to the UCL intensity. For the solid samples, the upconversion emission spectra excited at 791 nm are about 17–22 nm redshifted from photoluminescence spectra obtained at 396 nm excitation (Fig. 2 and Table I). Recent observations of UCL from CdTe quantum dots,^{14–16} as well as CdSe and InP quantum dots,^{14,15,17} show a similar redshift of the UCL spectrum relative to the PL spectrum. A model involving thermally populated surface or intra-band-gap states followed by resonant absorption has been used to explain the UCL process in these particles.

The dramatic shift in the UCL spectra of the solid samples relative to the PL spectra argues that surface or defect states may be involved in the UCL process in the solid samples. Both one- and two-photon absorption (PL and UCL, respectively) ultimately result in identical final

excitation energies; the fact that the UCL spectrum is redshifted argues that different subsets of particles are excited in each case. For instance, surface or defect states of slightly lower energy than the band edge may be preferentially excited in the two-photon excited upconversion relative to one-photon excitation because the excitation cross-section to these states may be greater. This effect can be enhanced in the solid particles as the surface capping is of lower quality because of the removal of capping agents during precipitation in acetone. Therefore, the UCL may selectively excite the most defected particles within the sample. The fact that the UCL power dependence is slightly smaller than two may be due to saturation of this subset. There is another possible cause of this redshift in the UCL spectrum relative to the PL spectrum. The UCL may be composed of luminescence from slightly larger particles, which would show redshifted luminescence. The two-photon excitation cross section to the larger particles may be slightly greater therefore, the UCL selectively displays this subset. Unfortunately, the experimental data do not allow a unique determination of the states involved in the upconversion in this case.

Our observations indicate that the upconversion luminescence in semiconductor nanoparticles is related to the quality, particularly surface characteristics. This is likely why different results are reported by different researchers. For the CdTe nanoparticles reported here, the upconversion is due to two-photon excitation. The demonstration of two-photon excitation for upconversion in nanoparticle solutions is of significant importance for applications, particularly for biological imaging, because two-photon optical imaging has several obvious advantages over fluorescence imaging.⁵ Two-photon excitation minimizes tissue photodamage, phototoxicity, and photobleaching as it limits the region of photointeraction to a subfemtoliter volume at the focal point. Two-photon excitation wavelengths are typically about double one-photon excitation wavelengths. This wide separation between excitation and emission spectra ensures that the excitation light and the Raman scattering can be rejected while filtering out a minimum of fluorescence photons. More importantly, advantages arise from the use of infrared wavelengths, thus avoiding tissue autofluorescence and increasing the tissue penetration depth.⁵

IV. SUMMARY

In summary, efficient upconversion luminescence from CdTe nanoparticles in solution and precipitated as solids has

been observed. The upconversion luminescence is shifted to longer wavelengths relative to the photoluminescence in the solid samples. The upconversion luminescence shows a non-linear near-quadratic power dependence at both room temperature and 10 K, leading to the conclusion that thermally populated surface states are not responsible for the upconversion. Instead, two-photon absorption is likely the dominant mechanism responsible for upconversion excitation in these samples.

ACKNOWLEDGMENTS

W.C. would like to thank Nomadics, Inc., the National Institute of Health (NIH, Grant No. 1 R43 CA112756-01

and No. 1R43CA110091-01), and the Department of Energy (DOE, Grant No. DE-FG02-04ER84023) for grants. Part of the research described in this paper was performed at the W.R. Wiley Environmental Molecular Sciences Laboratory, a national scientific user facility sponsored by the Department of Energy's Office of Biological and Environmental Research and located at the Pacific Northwest National Laboratory (PNNL). PNNL is operated by Battelle for the U.S. Department of Energy under Contract No. DE-AC06-76RLO1830. J.-O.M. and J.-O.B. would like to thank the Swedish Natural Science Research Council and the Foundation for Strategic Research of Sweden for financial support.

*Corresponding author. Electronic address: wchen@nomadics.com

¹E. Downing, L. Hesselink, J. Ralston, and R. M. Macfarlane, *Science* **273**, 1185 (1996).

²D. A. Parthenopoulos and P. M. Rentzepis, *Science* **245**, 843 (1989).

³M. P. Hehlen, H. U. Gudel, Q. Shu, and S. C. Rand, *J. Chem. Phys.* **104**, 1232 (1996).

⁴A. A. Said, C. Wamsely, D. J. Hagan, E. W. van Stryland, B. A. Reihardt, P. Roderer, and A. G. Dillard, *Chem. Phys. Lett.* **228**, 646 (1994).

⁵M. D. Cahalan, I. Parker, S. H. Wei, and M. J. Miller, *Nat. Rev. Immunology* **2**, 872 (2002).

⁶D. L. Petti, S. S. H. Wang, K. R. Gee, and G. J. Augustine, *Neuron* **19**, 465 (1997).

⁷F. Auzel, *Chem. Rev. (Washington, D.C.)* **104**, 139 (2004).

⁸W. Chen, A. G. Joly, and J. Z. Zhang, *Phys. Rev. B* **64**, 041202(R) (2001).

⁹L. A. Golovan, A. A. Goncharov, V. Y. Timoshenko, A. P. Shkurinov, P. K. Kashkarov, and N. I. Koroteev, *JETP Lett.* **68**, 770 (1998).

¹⁰J. Diener, D. Kovalev, H. Heckler, G. Polisski, N. Kunzner, F. Koch, Al. L. Efros, and M. Rosen, *Opt. Mater. (Amsterdam, Neth.)* **17**, 135 (2001).

¹¹N. Kunzner, D. Kovalev, H. Heckler, J. Diener, G. Polisski, F. Koch, Al. L. Efros, and M. Rosen, *Phys. Status Solidi B* **224**, 21 (2001).

¹²S. A. Blanton, A. Dehestani, P. V. Lin, and P. Guyot-Sionnest, *Chem. Phys. Lett.* **229**, 317 (1994).

¹³J. R. Lakowicz, I. Gryczynski, G. Piszczek, and C. J. Murphy, *J. Phys. Chem. B* **106**, 5365 (2002).

¹⁴Y. P. Rakovich, S. A. Filonovich, M. J. Gomes, J. F. Donegan, D. V. Talapin, A. L. Rogach, and A. Eychmuller, *Phys. Status Solidi B* **229**, 449 (2002).

¹⁵Y. P. Rakovich, A. A. Gladyschchuk, K. I. Rusakov, S. A. Filonovich, M. J. Gomes, D. V. Talapin, A. L. Rogach, and A. Eychmuller, *J. Appl. Spectrosc.* **69**, 444 (2002).

¹⁶X. Wang, W. Yu, J. Zhang, J. Aldana, X. Peng, and M. Xiao, *Phys. Rev. B* **68**, 125318 (2003).

¹⁷E. Poles, D. C. Selmarten, O. I. Micic, and A. J. Nozik, *Appl. Phys. Lett.* **75**, 971 (1999).

¹⁸K. I. Rusakov, A. A. Gladyschchuk, Y. P. Rakovich, J. F. Donegan,

S. A. Filonovich, M. J. Gomes, D. V. Talapin, A. L. Rogach, and A. Eychmuller, *Opt. Spectrosc.* **94**, 921 (2003).

¹⁹Y. P. Rakovich, J. F. Donegan, S. A. Filonovich, M. J. Gomes, D. V. Talapin, A. L. Rogach, and A. Eychmuller, *Physica E (Amsterdam)* **17**, 99 (2003).

²⁰C. Kammerer, G. Cassabois, C. Voisin, C. Delalande, and P. Roussignol, *Phys. Rev. Lett.* **87**, 207401 (2001).

²¹P. P. Paskov, P. O. Holtz, B. Monemar, J. M. Garcia, W. V. Schoenfeld, and P. M. Petroff, *Appl. Phys. Lett.* **77**, 812 (2000).

²²F. A. J. M. Driessen, *Appl. Phys. Lett.* **67**, 2813 (1995).

²³Z. P. Su, K. L. Teo, P. Y. Yu, and K. Uchida, *Solid State Commun.* **99**, 933 (1996).

²⁴M. Bruchez, M. Moronne, P. Gin, S. Weiss, and A. P. Alivisatos, *Science* **281**, 2013 (1998).

²⁵W. Chan and S. M. Nie, *Science* **281**, 2016 (1998).

²⁶B. Dubertret, P. Skourides, D. J. Norris, V. Noireaux, A. H. Brivanlou, and A. Libchaber, *Science* **298**, 1759 (2002).

²⁷S. Kim, Y. T. Lim, E. G. Soltesz, E. G. Soltesz, A. M. De Grand, J. Lee, A. Nakayama, J. A. Parker, T. Mihaljevic, R. G. Laurence, D. M. Dor, L. H. Cohn, M. G. Bawendi, and J. V. Frangioni, *Nat. Biotechnol.* **22**, 93, (2004).

²⁸B. Ballou, B. C. Lagerholm, L. A. Ernst, M. P. Bruchez, and A. S. Waggoner, *Bioconjugate Chem.* **15**, 79 (2004).

²⁹N. Morgan, S. English, W. Chen, V. Chernomordik, A. Russo, P. Smith, and A. Gandjbakhche, *Acad. Radiol.* **12**, 313 (2005).

³⁰N. Gaponik, D. Talapin, A. L. Rogach, K. Hoppe, E. V. Shevchenko, A. Kornowski, A. Eychmuller, and H. Weller, *J. Phys. Chem. B* **106**, 7177 (2002).

³¹D. Talapin, S. Haubold, A. L. Rogach, A. Kornowski, M. Haase, and H. Weller, *J. Phys. Chem. B* **105**, 2260 (2001).

³²W. Yu, Y. A. Wang, and X. Peng, *Chem. Mater.* **15**, 4300 (2003).

³³A. L. Rogach, L. Katsikas, A. Kornowski, D. Su, A. Eychmuller, and H. Weller, *Ber. Bunsenges. Phys. Chem.* **100**, 1772 (1996).

³⁴C. Kittel, in *Introduction to Solid State Physics*, 6th Edition (Wiley, New York, 1986), p. 185.

³⁵Y. A. I. Ekimov, Al. L. Efros, and A. A. Onuschenko, *Solid State Commun.* **56**, 921 (1985).

³⁶W. Chen, in *Handbook of Nanostructured Materials and Nanotechnology*, edited by H. S. Nalwa (Academic Press, San Diego, 2000).

³⁷*Handbook of X-Rays*, edited by E. F. Kaelble. (McGraw-Hill,

- New York, 1967).
- ³⁸D. R. Larson, W. R. Zipfel, R. M. Williams, S. W. Clark, M. P. Bruchez, F. W. Wise, and W. W. Webb, *Science* **300**, 1434 (2003).
- ³⁹S. F. Wuister, I. Swart, F. van Driel, S. G. Hickey, and C. de Mello Donega, *Nano Lett.* **3**, 503 (2003).
- ⁴⁰S. F. Wuister, F. van Driel, and A. Meijerink, *Phys. Chem. Chem. Phys.* **5**, 1253 (2003).
- ⁴¹G. Ghislotti, D. Ielmini, E. Riedo, M. Martinelli, and M. Della-giovanna *Solid State Commun.* **111**, 211 (1999).